# Temperature-activated polarization of single photon emitters

Haifa Jeridi, Sebastien Royer, Emmanuel Lhuillier, Emmanuelle Lacaze

▶ **To cite this version:**

Haifa Jeridi, Sebastien Royer, Emmanuel Lhuillier, Emmanuelle Lacaze. Temperature-activated polarization of single photon emitters. Applied Physics Letters, 2023, 123 (20), 10.1063/5.0169487 . hal-04304836

**HAL Id: hal-04304836**
**https://hal.science/hal-04304836v1**

Submitted on 24 Nov 2023

**HAL** is a multi-disciplinary open access archive for the deposit and dissemination of scientific research documents, whether they are published or not. The documents may come from teaching and research institutions in France or abroad, or from public or private research centers.

L'archive ouverte pluridisciplinaire **HAL**, est destinée au dépôt et à la diffusion de documents scientifiques de niveau recherche, publiés ou non, émanant des établissements d'enseignement et de recherche français ou étrangers, des laboratoires publics ou privés.

# Temperature-activated polarization of single photon emitters

Haifa Jeridi,[1,2] Sebastien Royer,[2] Emmanuel Lhuillier,[2] and Emmanuelle Lacaze[2]
[1)]*ECE Research Center (LyRIDS), ECE Engineering School, 75015 Paris, France.*
[2)]*CNRS, Institut des Nanosciences de Paris, INSP, Sorbonne Université, F-75005 Paris, France.*

(*Electronic mail: emmanuelle.lacaze@insp.jussieu.fr.)

(Dated: 24 November 2023)

Controlled activation of the polarization of single photon emitters is a challenge. We use CdSe/CdS dot-in-rods (DRs) confined and oriented in smectic topological grain boundaries to activate the fluorescence polarization through temperature variation. We show that temperature acts as a knob to switch on/off the polarization of DR emitted light between smectic and isotropic phase. This occurs through the orientational motion of the DR assemblies that occurs in isotropic phase in relation to the disappearing of the defects. In addition, we evidence a significant improvement of DR emitted light polarization after cooling back from the isotropic phase. It is measured by the increase of polarization degree from 0.28 to 0.36 on average for DR assemblies. This improvement appears managed by the smectic phase diagram near the smectic/nematic transition. Near the smectic/nematic transition the smectic grain boundaries entirely cover the sample surface and allow for a re-orientation of all DRs, even of those initially not confined in smectic grain boundaries.

Random distribution of nanorods orientation fully obviates their unusual anisotropic optical properties. Materials inherit the microscopic anisotropic features of nanorods only if the rods can be oriented along a single direction throughout the entire sample. This concerns for example Localized Surface Plasmon Resonance (LSPR) for metallic nanorods and fluorescence polarization for semi-conducting nanorods. Several tools now exist to orient colloidal nanorods initially synthesized in solution. For example, the solvent evaporation can be controlled.[1–4] Template-assisted colloidal self-assembly can be performed.[5–7] For other shapes (nanoplatelets) it has also been shown that coupling to a plasmonic grating can impose the polarization of HgTe nanoplatelets.[8] However, if the nanorods are not embedded in an active matrix like liquid crystals, it remains difficult to activate their polarization by an external parameter. Activating the polarization of semiconducting nanorods requires a controlled reconfiguration of the orientation or/and organization of the nanorods by an external parameter.[1] In this context, liquid crystal matrices are attractive because of their ability to be easily modified by an electric or magnetic field or when temperature varies. In nematic phase, proper functionalization of colloidal nanorods can induce well-defined orientation of the long rod axis with respect to the nematic director.[9] Within nematic cells, the electric field induces, together with the nematic director reorientation, the reorientation of colloidal nanorods. This leads to LSPR for gold nanorods[10] and fluorescence polarization for rod-shaped upconversion nanoparticles[11] controlled by an electric field. Exploring the use of a different external parameter like temperature is now interesting, also to test if different changes of optical properties can be obtained.

It is known that long colloidal nanorods can form nematic phases in solution when the concentration is high enough.[12] However, the temperature does not significantly influence their structure, nanorods being mostly reoriented by magnetic or electric field.[13] Temperature-driven phase transitions have been evidenced for nanorods of aspect ratio between 40 and 110 when they are mixed with nematic molecules.[14] For small metallic nanorods displaying LSPR absorption in the visible range or for fluorescent nanorods that could emit polarized light, eventually as single photon emitters, an interesting alternative could be the confinement of nanorods within oriented liquid crystal topological defects. These defects would indeed disappear during liquid crystal phase transitions driven by temperature.

The release of the LC defect energy allows for the stabilization of a composite system in the presence of nanoparticles when they are confined in the defect cores.[15–21] LC topological defects may thus be used as a matrix for different types of nanoparticle organizations templated by the defect geometry[19,22,23] provided that the defects are well-oriented. The influence of temperature on nanorod organization below the nematic/isotropic phase transition has been recently studied, both theoretically and experimentally for nanorods confined and oriented by twist disclinations.[24] Reversible modifications of optical properties of nanorods have been obtained at the smectic/nematic phase transition with gold nanorods initially organized in arrays of smectic focal conics.[25] We here propose a comprehensive picture of the relationship between evolution of nanorod organization and the evolution of temperature-induced fluorescence polarization. It has been studied when the temperature is switched on/off between smectic phase and 50 °C isotropic phase in relation to the presence of topological grain boundaries in smectic phase. This analysis has been performed with CdSe-CdS dot-in-rods (DRs of diameter 7 nm and length 22 nm) - single photon emitters - of fluorescence polarization parallel to their long axis.[26]

We have worked with the smctic 4-*n*-octyl-4'-cyanobiphenyl (8CB) which displays two phase transitions, the smectic/nematic phase transition at 33.5°C and the nematic/isotropic phase transition at 40.5°C. We have prepared thin 8CB films of thickness ranging between 150 and 250 nm. There are two kinds of coexisting smectic textures at room temperature[27] (Fig. 1), 60% of oily streaks ((OSs), Fig. 1(b)) and 40% of the so-called large stripes ((LSs), Fig. 1(d)). Both textures form parallel stripes along (Ox) axis (Fig. 1(c)) that can be identified by Polarized Optical

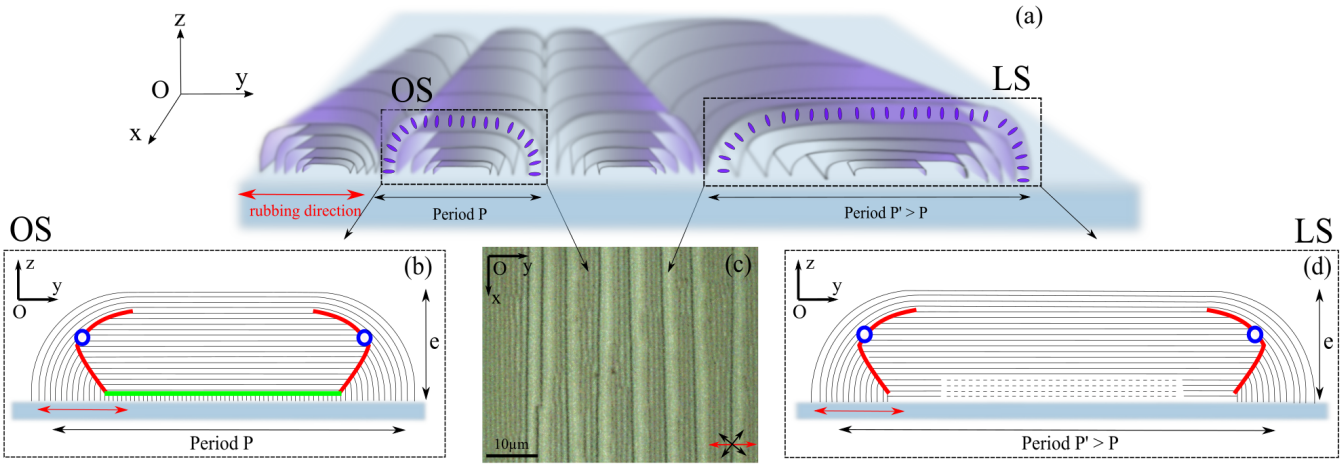


FIG. 1. (a) Simplified 3D schematic of the flattened hemicylinders formed by the curved smectic layers, with the molecular orientation shown in purple, Oily Streaks (OSs) on the left and Large Stripes (LSs) on the right. ((b) and (d)) Cross-sectional views ((Oyz) plane) of one hemicylinder of an OS texture and a LS texture, respectively; (b) The OS internal structure with superimposed smectic layers, two rotating grain boundaries in red (including linear dislocations in blue) and a 2D central defect in green; (d) similar expected architecture for the LS structure at the edges but with a larger periodicity associated with the absence of a central defect. (c) Microscopic picture in reflection between crossed polarizers showing the top view ((Oxy) plane) of a smectic film (thickness $e \approx 200$ nm; around 60% of OSs and 40% of LS).

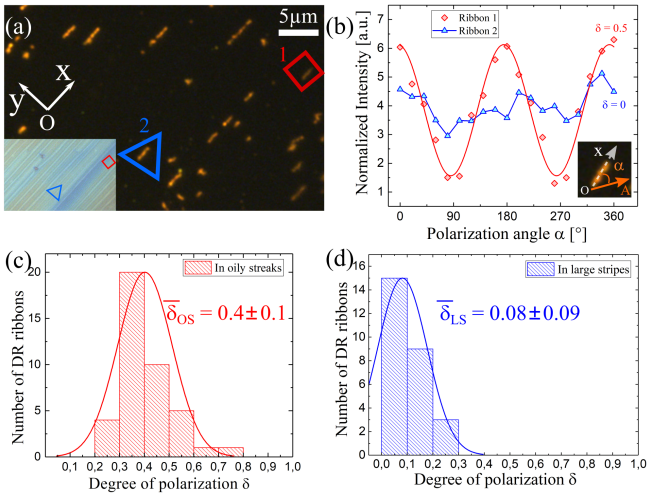


FIG. 2. (a) Fluorescent microscopy picture of a DRs/8CB film area of local concentration $c_{avg} = 185$ DRs $\mu$m$^{-2}$ and LC thickness $e \approx 173$ nm with the inset showing the corresponding POM picture taken in reflection between parallel polarizers. The red square and the blue triangle enclose DR ribbons respectively formed in an OS (ribbon #1) and a LS (ribbon #2). (b) Evolution of the photoluminescence intensities per unit of area with the analyzer orientation $\alpha$ for DRs ribbon #1 and DR ribbon #2 (Fig. 2(a)), $\alpha = 0°$ corresponding to the direction of the 8CB stripes (Ox). Both curves are offsetted for comparison. The intensity profiles of ribbon #1 is fitted with the function $I_{min} + (I_{max} - I_{min})\cos^2(\alpha)$, leading for ribbon #1 to a polarization degree $\delta = (I_{max} - I_{min})/(I_{max} + I_{min}) = 0.5$. (c) and (d) The histograms of polarization degrees respectively measured with 53 ribbons in OSs and 27 ribbons in LSs. The histograms are fitted with gaussians to extract the average polarization degrees, $\overline{\delta}_{OS}$ and $\overline{\delta}_{LS}$.

Microscopy (POM).[28] They appear due to antagonistic anchoring between the two interfaces of the thin film. On the substrate, planar unidirectional anchoring is provided by poly-vinyle (PVA) polymer rubbed along (Oy) direction. Smectic layers with their normal parallel to (Oy) are thus favored on the substrate. At the air interface, there is a homeotropic anchoring leading to smectic layers of normal parallel to (Oz). The smectic layers become superimposed into periodic flattened hemicylinders corresponding to the stripes detected by POM along the (Ox) axis. OSs of period $P$ between 0.5 $\mu$m and 1 $\mu$m are preferred with strong anchoring strength. They present a central ribbon-like topological grain boundary that connects the smectic layers perpendicular to the PVA substrate to flat layers (in green in Fig. 1(b)) in the center of the hemicylinders.[29] Fluorescent DRs, when mixed with 8CB OSs in thin films (100-300 nm), become confined in the grain boundaries.[27] They form elongated ribbons localized in the central defects and parallel to (Ox) axis - see ribbon #1 (red square) of Fig. 2(a). These ribbons emit light of polarization parallel to their long axis and to the 8CB stripes. This is shown by the sinusoidal shape of the emitted intensity as a function of the analyzer orientation $\alpha$ (Fig. 2(b)). It is maximum at $\alpha$ = 0, along (Ox) axis. The ribbons are thus made of DRs in average parallel to the 8CB stripes. This is most probably due to the coupling between DRs and the perpendicular smectic layers below the grain boundaries, all parallel to (Ox) axis.[27] Some disorder of DR orientation is observed within the ribbons as demonstrated by the polarization degree $\delta = (I_{max} - I_{min})/(I_{max} + I_{min}) = 0.5$ for ribbon #1( Fig. 2(b)), smaller than the one for single DRs, around 0.6.[30] The polarization degree histogram for 53 DR ribbons in smectic OSs is shown in Fig. 2(c) leading to an average polarization degree value $\overline{\delta}_{OS} = 0.4 \pm 0.1$.[27] LSs of period, $P$', between 1 $\mu$m and 3 $\mu$m are preferred with weaker

anchoring strength. The anchoring strength thus controls the respective proportion of OSs and LSs in smectic films (Fig. 1(c)).[27] For LSs ellipsometric measurements suggest the absence of grain boundaries.[27] As a result, the fluorescent ribbons formed within LSs parallel to (Ox), are non-polarized (ribbon #2 (blue triangle) of Fig. 2(a)-(b)), in relation with a disordered orientation of DRs within the ribbons.[27] The polarization degree histogram for 27 DR ribbons in LSs leads to an average value $\overline{\delta}_{LS} = 0.08 \pm 0.1$ (Fig. 2(c)).

We applied an annealing process by abruptly increasing the temperature from room temperature to 50 °C, above the isotropic phase transition. The transition to the nematic phase is thus fast and only leads to small fluctuations around the (Oz) axis. It is thus expected to preserve the average polarization of the ribbons with possibly a slightly reduced average polarization degree. Even in the isotropic phase at 50 °C, the DRs ribbons preserve their elongated shape as shown in Fig. 3(a). However they are no longer oriented along (Ox), the initial orientation of the smectic defects (Fig. 1(a)). Due to the disappearance of the smectic topological defects and to the fluidity of the isotropic phase, they are now able to rotate around the (Oz) axis, while maintaining their ribbon-like shape. The angle $\varphi$ between the ribbon long axis and (Ox) varies with time between 0 and 180° (Fig. 3(b)). For some ribbons, like the one shown in Fig. 3(b), the emitted light intensity for a fixed analyzer orientation along (Ox) is accordingly no more constant. The time-averaged emission of this ribbon is therefore not polarized. Since the fluctuations of the ribbon orientations are not correlated throughout the sample, the instantaneous light emitted by the overall sample also becomes non polarized. Based on these results, temperature can be used as an external parameter to control the average light polarization of the composite.

In order to explore the corresponding evolution of the DRs organization within the ribbons in isotropic phase, we have analyzed the polarization of the emitted light of the fluorescent ribbon shown in Fig 3(b). For such a purpose we have drawn the emitted intensity as a function of the ribbon long axis orientation $\varphi$ (Fig. 3(c)), keeping the analyzer fixed parallel to (Ox). If the DRs organization is fully disordered within the ribbon, the emitted intensity would be constant in the presence of the analyzer. This was the case of the DRs ribbons formed in LSs at room temperature (Fig. 2(b)). However, this is not the case for the ribbon shown in Fig. 3(b). The clear maximum of the corresponding emitted intensity at $\varphi = 0°$, shown in Fig. 3(c), demonstrates that in one given ribbon the DRs orientation is not fully disordered. The average DRs orientation remains parallel to the ribbon long axis, like it was before heating. The corresponding effective polarization degree is $\delta_{iso} = 0.32$. The $\delta_{iso}$ histogram for 26 ribbons shown in Fig. 3(d) displays values ranging from 0 to 0.4. They lie in between OS and LS values of the smectic film at room temperature (Fig. 2(c) and (d)). This is partly since the ribbons measured in isotropic phase are indistinctly chosen between ribbons initially formed at room temperature in OSs or in LSs. However, the proportion of polarization degrees around 0 appears larger than the 40% proportion of LSs within the 8CB thin films. Moreover, there is no $\delta$ value larger than 0.4 in

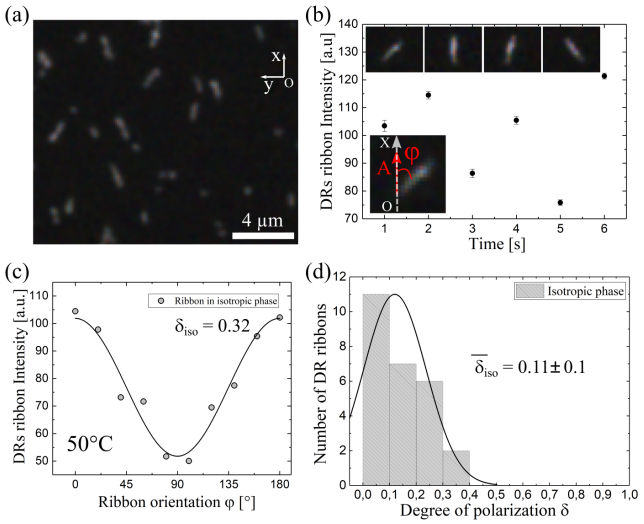


FIG. 3. (a) Fluorescent microscopy picture of a DRs/8CB film area in isotropic phase (50 °C). (b) The photoluminescence intensity evolution with time of a DRs ribbon shown in the inset when the analyzer is fixed parallel to (Ox). (c) Evolution of the photoluminescence intensity per unit of area with the angle $\varphi$ between the analyzer (Ox) and the DR ribbon long axis (see inset of Fig. 3(b)), leading to a degree of polarization $\delta = 0.32$. (d) Histogram of the degrees of polarization measured for 26 DR ribbons in 8CB isotropic phase. The histogram is fitted with a gaussian curve to extract $\overline{\delta}_{iso} = 0.11 \pm 0.1$.

contrast with the values shown on the histogram of Fig. 2(c). The disorder of DR ribbons initially formed in OSs may thus increase when the isotropic phase is reached. This occurs with an average orientation of the DRs always preserved parallel to the ribbon's long axis.

In a second step, we have studied the fluorescent ribbons back in the smectic phase after the above presented annealing in isotropic phase. After at least one minute in isotropic phase, the hot plate has been stopped, leading to a slow decrease of temperature back to room temperature. The initial smectic association of OSs and LSs is recovered back at room temperature with almost the same respective proportion of 40% and 60% (inset of Fig. 4(a)). Fluorescent ribbons are still observed but all with their long axis parallel to (Ox), the 8CB stripes axis (Fig. 4(a)), in contrast with the observation in isotropic phase (Fig. 3(a)) but similarly to the initial orientation observed before annealing (Fig. 2(a)). In OSs, the polarization of emitted light is still parallel to the ribbon long axis (Ox) which is the 8CB stripes direction (maximum of emitted light at $\alpha = 0°$ for ribbon #3 (red square) of Fig. 4(a)-(b)). The histograms of polarization degree after annealing for 33 DR ribbons trapped in OSs and for 36 DR ribbons trapped in LSs are presented in Fig. 4(c) and (d). For OSs the histogram with an average value $\overline{\delta}_{OS} = 0.38 \pm 0.06$ after annealing (Fig. 4(c)) appears similar to the one of Fig. 2(c) obtained in OSs before the annealing process ($\overline{\delta}_{OS} = 0.4 \pm 0.06$). However, the histogram of LSs surprisingly changed with an average polarization degree no more zero (Fig. 4(d)). For most ribbons in LSs, the emitted intensity in presence of an analyzer now

displays a well-defined sinusoidal shape with a maximum of emitted intensity at $\alpha = 0°$, parallel to the stripes (ribbon #4 (blue triangle) of Fig. 4(a)-(b)). The corresponding average polarization degree displayed by the histogram of Fig. 4(d) is $\overline{\delta}_{LS} = 0.34 \pm 0.13$ close to $\overline{\delta}_{OS} = 0.38 \pm 0.06$ for OSs (Fig. 4(c)). As a result, the polarization of light of the overall sample is significantly better defined. Now all ribbons emit light of similar polarization, parallel to 8CB stripes. The overall average polarization degree become $\overline{\delta}_{after} = 0.36$. Before annealing only ribbons in OSs (60% of the ribbons) displayed polarized light with a polarization degree of average 0.4. The overall polarized light has thus increased from $\overline{\delta}_{before} = 0.24$ before annealing to $\overline{\delta}_{after} = 0.36$ after annealing. After a second annealing, the DR ribbon polarization no more notably varies.

In these composites of oriented defects and fluorescent DRs, temperature can be viewed as a knob allowing firstly to switch on/off the average polarization of emitted light of the overall sample ($\overline{\delta}$ from 0.24 to 0 then from 0 to 0.36). Secondly, temperature may be viewed as a parameter allowing to increase the polarized light at room temperature after annealing ($\overline{\delta}$ from 0.24 before annealing to 0.36 after annealing). At high temperatures in isotropic phase (50 °C), the emitted light becomes non-polarized due to the orientational motion of the fluorescent ribbons. However, the ribbons preserve their isotropic shape and their integrity with a constant intensity and thus a constant number of DRs packed within the ribbons. For one given ribbon DRs don't get spread in the surrounding isotropic phase. This is due to the Van der Waals interactions between DRs that have occurred during their initial formation in smectic phase. In isotropic phase for DR ribbons initially formed within OSs Van der Waals interactions can even preserve the average orientation of the DRs parallel to the ribbon long axis, as shown by Fig. 3(c). However, the observed average polarization degree decreases (Fig. 3(d)) with respect to smectic phase (Fig. 2(c)-(d)) reveals some enhanced disorder within the ribbons. It is known that Van der Waals interactions between neighboring nanoparticles are mostly mediated by the interactions between the interdigitated ligands.[31,32] The temperature increase may have led to some ligand disorder and thus to decreased Van der Waals interactions between DRs.

Why are the ribbons from LSs well-oriented after cooling back in the smectic phase? To understand it, we have followed by POM the appearance and evolution of OSs when temperature is decreased from the nematic/smectic phase transition (around 33.5 °C). Fig. 5(d) corresponds to a 8CB area with around 40% of LSs at room temperature. Just after phase transition in smectic phase, almost only OSs are observed (Fig. 5(a)). LSs appear at a temperature around 0.5 °C below. Their proportion then increases when temperature is decreased (Fig. 5(a)-(d)). This evolution is a signature of a larger number of topological defects in OSs with respect to LSs, of energy increasing when temperature difference with nematic/smectic phase transition increases. This observation suggests that all fluorescent ribbons may become confined within the defects of OSs at the nematic/smectic phase transition when LSs are still absent. DRs of all ribbons may thus become reorganized within OSs and oriented by their coupling with the oriented smectic layers below the OS central grain boundaries.[27] Once formed in the OS at the smectic/nematic transition, the ribbons remain oriented if they are finally trapped in a LS during cooling to room temperature. Ribbons initially formed in OSs before annealing will be tilted to become parallel to the stripes and only small re-organization of the already oriented DRs within the ribbons is induced. In contrast, ribbons made

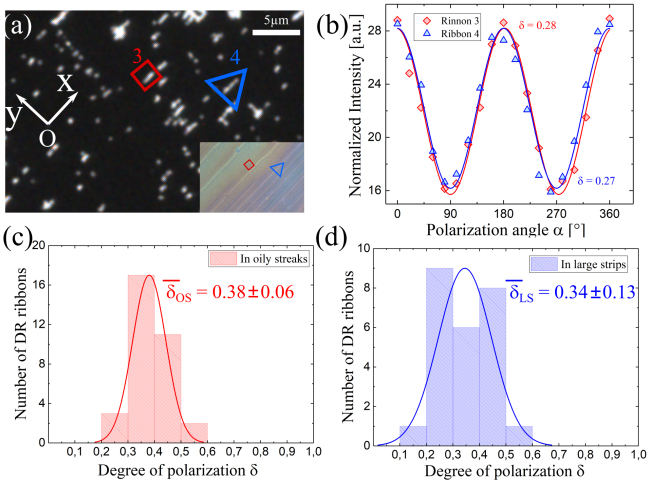


FIG. 4. (a) Fluorescent microscopy picture of a DRs/8CB film area of a local concentration $c_{avg} = 185$ DRs $\mu$m$^{-2}$ and LC thickness $e \approx 230$ nm, after annealing. The inset shows the corresponding POM picture taken in reflection between parallel polarizers. The red square and the blue triangle enclose DR ribbons respectively within an OS (ribbon #3) and a LS (ribbon #4). (b) Evolution of the photoluminescence intensities per unit of area with the analyzer orientation $\alpha$ of ribbon #3 and ribbon #4 (Fig. 2(a)) respectively, leading to $\delta = 0.28$ for both. The curves are offsetted to allow for a comparison on the same graph. (c) and (d) The histograms of the degrees of polarization respectively measured with 33 ribbons in OS and 36 ribbons in LS. The histograms are fitted with gaussians to extract the average polarization degrees, $\overline{\delta}_{OS} = 0.38 \pm 0.06$ and $\overline{\delta}_{LS} = 0.3 \pm 0.13$.

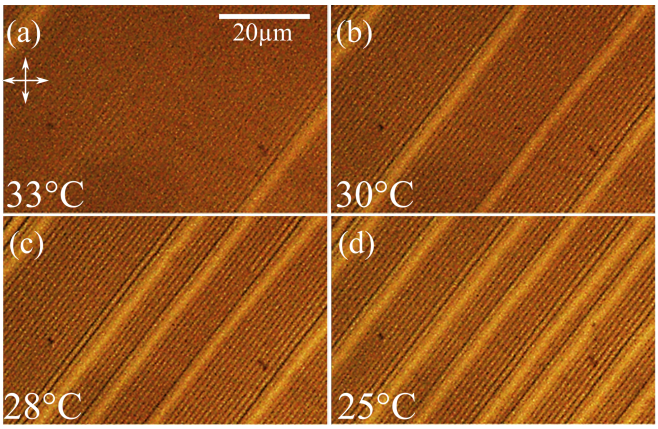


FIG. 5. POM images between crossed polarizers showing the OSs transformation into LSs after the nematic-smectic transition: (a) at $T$ =33 °C, (b) at $T$ =30 °C, (c) at $T$ =28 °C and (d) at $T$ =25 °C.

of disordered DRs, initially formed in LSs before annealing, will undergo a large re-organization of the DRs within the ribbons at the smectic/nematic transition. This latter feature may be possible due to the reduction in Van der Waals interactions between neighboring DRs that have occurred at high temperatures. This result also confirms the large coupling that may occur between DRs confined in smectic grain boundaries and the perpendicular layers below the grain boundaries,[27] able to lead to a re-orientation of DRs within ribbons.

In conclusion, we demonstrate two efficient ways by which temperature allows for the control of fluorescence polarization of single photon emitters CdS-CdSe DRs in relation to a control of their organization within smectic textures. For such a purpose we use a mixture of polarized and non-polarized DR ribbons formed respectively within topological grain boundaries of oily streaks (OSs) and within large stripes (LSs) in the absence of grain boundaries. Firstly, the disappearing of the grain boundaries in isotropic phase together with the fluidity of the isotropic phase at 50 °C induces a rotational motion of the DR ribbons initially strictly oriented in smectic phase. The fluorescence of the DRs becomes non-polarized on average in isotropic phase. After cooling back in smectic phase, the fluorescence polarization in OSs is recovered. Temperature thus acts as a switch on/off for fluorescence polarization of DRs confined in OSs. Secondly, the temperature driven smectic phase diagram appears associated with a domination of OSs with respect to LSs at the cooling back close to nematic/smectic phase transition. When DR ribbons reorient parallel to the 8CB stripes in smectic phase, the reorganization of DRs within the ribbons is first controlled by OS grain boundaries. All DRs can thus become guided by the smectic layers below the grain boundaries and consequently orient in average parallel to the ribbon axis and to the 8CB stripes. This reorganization appears possible thanks to a decrease in Van der Waals interactions between the DRs of a given ribbon initiated in isotropic phase. All DR ribbons at room temperature, both in OSs and in LSs, become polarized after annealing in isotropic phase. An enhancement of the average polarization degree is thus reached from 0.24 to 0.36 after annealing. Such temperature-induced activation of single-photon emitters could also be applied to different kinds of anisotropic nanoparticles. For example, it could be implemented for pyramid/bipyramid of CdSe-CdS, which exhibit high photoluminescence and significant suppressed blinking[33] or for CdSe-CdS dot-in-plate.[34] The use of metallic nanoparticles such as plasmonic nanorods,[35] nanoplates[36] or bipyramids[37] can alternatively raise the potential technological utility of our demonstrated approach.

## SUPPLEMENTARY MATERIAL

See supplementary material for more information about the experimental setup (synthesis of DRs, sample preparation, and optical and fluorescence microscopy techniques).

## ACKNOWLEDGMENTS

We thank Laurent Coolen for the useful discussions.

## AUTHOR DECLARATION

### Conflict of interest

The authors have no conflicts to disclose.

### Author contributions

Conceptualization, methodology, visualization, resources: Haifa Jeridi, Sebstien Royer, Emmanuel Lhuillier, and Emmanuelle Lacaze. Writing original draft, review and editing: Haifa Jeridi and Emmanuelle Lacaze. Data creation, formal analysis: Haifa Jeridi. Funding acquisition, project administration, supervision, validation: Emmanuelle Lacaze.

## DATA AVAILABILITY STATEMENT

The data that support the findings of this study are available from the corresponding author upon reasonable request.

## REFERENCES

[1]X. Ye, C. Zhu, P. Ercius, S. N. Raja, B. He, M. R. Jones, M. R. Hauwiller, Y. Liu, T. Xu, and A. P. Alivisatos, "Structural diversity in binary superlattices self-assembled from polymer-grafted nanocrystals," Nature communications **6**, 10052 (2015).

[2]C. Hamon, M. Postic, E. Mazari, T. Bizien, C. Dupuis, P. Even-Hernandez, A. Jimenez, L. Courbin, C. Gosse, F. Artzner, *et al.*, "Three-dimensional self-assembling of gold nanorods with controlled macroscopic shape and local smectic b order," ACS nano **6**, 4137–4146 (2012).

[3]B. T. Diroll, N. J. Greybush, C. R. Kagan, and C. B. Murray, "Smectic nanorod superlattices assembled on liquid subphases: structure, orientation, defects, and optical polarization," Chemistry of Materials **27**, 2998–3008 (2015).

[4]Y. Liang, Y. Xie, D. Chen, C. Guo, S. Hou, T. Wen, F. Yang, K. Deng, X. Wu, I. I. Smalyukh, *et al.*, "Symmetry control of nanorod superlattice driven by a governing force," Nature communications **8**, 1–8 (2017).

[5]C. Hanske, M. Tebbe, C. Kuttner, V. Bieber, V. V. Tsukruk, M. Chanana, T. A. F. Konig, and A. Fery, "Strongly coupled plasmonic modes on macroscopic areas via template-assisted colloidal self-assembly," Nano Lett. **14**, 6863–6871 (2014).

[6]V. Flauraud, M. Mastrangeli, G. D. Bernasconi, J. Butet, D. T. Alexander, E. Shahrabi, O. J. Martin, and J. Brugger, "Nanoscale topographical control of capillary assembly of nanoparticles," Nature nanotechnology **12**, 73–80 (2017).

[7]C. Matricardi, C. Hanske, J. L. Garcia-Pomar, J. Langer, A. Mihi, and L. M. Liz-Marzan, "Gold nanoparticle plasmonic superlattices as surface - enhanced raman spectroscopy substrates," ACS Nano **12**, 8531–8539 (2018).

[8]C. Dabard, E. Bossavit, T. H. Dang, N. Ledos, M. Cavallo, A. Khalili, H. Zhang, R. Alchaar, G. Patriarche, A. Vasanelli, B. T. Diroll, A. Degiron, E. Lhuillier, and S. Ithurria, "Electroluminescence and plasmon-assisted directional photoluminescence from 2d hgte nanoplatelets," The Journal of Physical Chemistry C **127**, 14847–14855 (2023).

[9]B. Senyuk, C. Meng, and I. I. Smalyukh, "Design and preparation of nematic colloidal particles," Langmuir **38**, 9099–9118 (2022).

[10]Q. Liu, Y. Yuan, and I. I. Smalyukh, "Electrically and optically tunable plasmonic guest–host liquid crystals with long-range ordered nanoparticles," Nano letters **14**, 4071–4077 (2014).
[11]H. Mundoor and I. I. Smalyukh, "Mesostructured composite materials with electrically tunable upconverting properties," Small **11**, 5572–5580 (2015).
[12]L. Onsager, "Unique orientation of 1d and 2d nanoparticle assemblies confined in smectic topological defects," Ann. N.Y. Acad. Sci. **51**, 627 (1949).
[13]S. Park, H. Mundoor, B. Fleury, P. Davidson, J. van de Lagemaat, and I. I. Smalyukh, "Liquid crystalline order and electric switching of upconversion luminescence in colloidal nanorod suspensions," Advanced Optical Materials **7**, 1900041 (2019).
[14]H. Mundoor, S. Park, B. Senyuk, H. H. Wensink, and I. I. Smalyukh, "Hybrid molecular-colloidal liquid crystals," Science **360**, 768–771 (2018).
[15]H. Yoshida, Y. Tanaka, K. Kawamoto, H. Kubo, T. Tsuda, A. Fujii, S. Kuwabata, H. Kikuchi, and M. Ozaki, "Nanoparticle-stabilized cholesteric blue phases," Applied physics express **2**, 121501 (2009).
[16]E. Karatairi, B. Rožič, Z. Kutnjak, V. Tzitzios, G. Nounesis, G. Cordoyiannis, J. Thoen, C. Glorieux, and S. Kralj, "Nanoparticle-induced widening of the temperature range of liquid-crystalline blue phases," Physical Review E **81**, 041703 (2010).
[17]B. Rožič, V. Tzitzios, E. Karatairi, U. Tkalec, G. Nounesis, Z. Kutnjak, G. Cordoyiannis, R. Rosso, E. G. Virga, I. Muševič, *et al.*, "Theoretical and experimental study of the nanoparticle-driven blue phase stabilisation," The European Physical Journal E **34**, 1–11 (2011).
[18]B. Senyuk, J. S. Evans, P. J. Ackerman, T. Lee, P. Manna, L. Vigderman, E. R. Zubarev, J. van de Lagemaat, and I. I. Smalyukh, "Shape-dependent oriented trapping and scaffolding of plasmonic nanoparticles by topological defects for self-assembly of colloidal dimers in liquid crystals," Nano letters **12**, 955–963 (2012).
[19]J. S. Evans, P. J. Ackerman, D. J. Broer, J. van de Lagemaat, and I. I. Smalyukh, "Optical generation, templating, and polymerization of three-dimensional arrays of liquid-crystal defects decorated by plasmonic nanoparticles," Physical Review E **87**, 032503 (2013).
[20]G. Cordoyiannis, V. S. R. Jampani, S. Kralj, S. Dhara, V. Tzitzios, G. Basina, G. Nounesis, Z. Kutnjak, C. S. P. Tripathi, P. Losada-Pérez, *et al.*, "Different modulated structures of topological defects stabilized by adaptive targeting nanoparticles," Soft matter **9**, 3956–3964 (2013).
[21]D. S. Kim, A. Honglawan, S. Yang, and D. K. Yoon, "Arrangement and sers applications of nanoparticle clusters using liquid crystalline template," ACS applied materials & interfaces **9**, 7787–7792 (2017).
[22]M. A. Gharbi, S. Manet, J. Lhermitte, S. Brown, J. Milette, V. Toader, M. Sutton, and L. Reven, "Reversible nanoparticle cubic lattices in blue phase liquid crystals," ACS nano **10**, 3410–3415 (2016).
[23]H. Mundoor, G. H. Sheetah, S. Park, P. J. Ackerman, I. I. Smalyukh, and J. van de Lagemaat, "Tuning and switching a plasmonic quantum dot "sandwich" in a nematic line defect," ACS nano **12**, 2580–2590 (2018).
[24]M. Tasinkevych, S. Park, H. Mundoor, and I. I. Smalyukh, "Nanoparticle localization within chiral liquid crystal defect lines and nanoparticle interactions," Physical Review E **107**, 034701 (2023).
[25]E. Lee, Y. Xia, R. C. Ferrier Jr, H.-N. Kim, M. A. Gharbi, K. J. Stebe, R. D. Kamien, R. J. Composto, and S. Yang, "Fine golden rings: tunable surface plasmon resonance from assembled nanorods in topological defects of liquid crystals," Advanced Materials **28**, 2731–2736 (2016).
[26]F. Pisanello, L. Martiradonna, G. Leménager, P. Spinicelli, A. Fiore, L. Manna, J.-P. Hermier, R. Cingolani, E. Giacobino, M. De Vittorio, *et al.*, "Room temperature-dipolelike single photon source with a colloidal dot-in-rod," Applied Physics Letters **96** (2010).
[27]H. Jeridi, J. de Dieu Niyonzima, C. Sakr, A. Missaoui, S. Shahini, A. Vlad, A. Coati, N. Goubet, S. Royer, I. Vickridge, *et al.*, "Unique orientation of 1d and 2d nanoparticle assemblies confined in smectic topological defects," Soft Matter **18**, 4792–4802 (2022).
[28]J.-P. Michel, E. Lacaze, M. Goldmann, M. Gailhanou, M. De Boissieu, and M. Alba, "Structure of smectic defect cores: X-ray study of 8cb liquid crystal ultrathin films," Physical review letters **96**, 027803 (2006).
[29]D. Coursault, B. Zappone, A. Coati, A. Boulaoued, L. Pelliser, D. Limagne, N. Boudet, B. H. Ibrahim, A. De Martino, M. Alba, *et al.*, "Self-organized arrays of dislocations in thin smectic liquid crystal films," Soft Matter **12**, 678–688 (2016).
[30]L. Pelliser, M. Manceau, C. Lethiec, D. Coursault, S. Vezzoli, G. Leménager, L. Coolen, M. DeVittorio, F. Pisanello, L. Carbone, *et al.*, "Alignment of rod-shaped single-photon emitters driven by line defects in liquid crystals," Advanced Functional Materials **25**, 1719–1726 (2015).
[31]P. Schapotschnikow, R. Pool, and T. J. Vlugt, "Molecular simulations of interacting nanocrystals," Nano letters **8**, 2930–2934 (2008).
[32]S.-P. Do, A. Missaoui, A. Coati, D. Coursault, H. Jeridi, A. Resta, N. Goubet, M. M. Wojcik, A. Choux, S. Royer, *et al.*, "From chains to monolayers: Nanoparticle assembly driven by smectic topological defects," Nano Letters **20**, 1598–1606 (2020).
[33]R. Tan, Y. Yuan, Y. Nagaoka, D. Eggert, X. Wang, S. Thota, P. Guo, H. Yang, J. Zhao, and O. Chen, "Monodisperse hexagonal pyramidal and bipyramidal wurtzite cdse-cds core–shell nanocrystals," Chemistry of Materials **29**, 4097–4108 (2017).
[34]E. Cassette, B. Mahler, J.-M. Guigner, G. Patriarche, B. Dubertret, and T. Pons, "Colloidal cdse/cds dot-in-plate nanocrystals with 2d-polarized emission," ACS nano **6**, 6741–6750 (2012).
[35]B. Rozic, J. Fresnais, C. Molinaro, J. Calixte, S. Umadevi, S. Lau-Truong, N. Felidj, T. Kraus, F. Charra, V. Dupuis, *et al.*, "Oriented gold nanorods and gold nanorod chains within smectic liquid crystal topological defects," ACS nano **11**, 6728–6738 (2017).
[36]S. Ghosh and I. Smalyukh, "Electrical switching of nematic plasmonic nanocolloids for infrared solar gain control," Advanced Optical Materials **10**, 2201513 (2022).
[37]Z. Mai, Y. Yuan, J.-S. B. Tai, B. Senyuk, B. Liu, H. Li, Y. Wang, G. Zhou, and I. I. Smalyukh, "Nematic order, plasmonic switching and self-patterning of colloidal gold bipyramids," Advanced Science **8**, 2102854 (2021).